J. Phys. IV France **8** (1998)

On size effects in torsion of multi- and polycrystalline specimens

S. Quilici, S. Forest and G. Cailletaud

École des Mines de Paris, Centre des Matériaux, UMR 7633 du CNRS, BP. 87, 91003 Evry, France

Abstract : Simulations of torsion of copper single, multi- and polycrystals are presented. The stress is laid on an accurate description of intragranular behaviour, which requires the use of parallel computing. If the wire contains up to 1000 grains, the deformation is shown to localize within some weak sections of the specimen. A lower bound of a critical grain number for a multi- to polycrystal plasticity transition is therefore established.

1 INTRODUCTION

Experimental results of the torsion of copper wires of different diameters and two given grain sizes have been provided in [1]. Significant size effects have been reported, the thinnest wires displaying the strongest response. For the latter specimen, the section of each specimen contains only 4 to 5 grains. The modeling of these tests proposed in [1] is an enhancement of Mises-type plasticity. According to us, the interpretation of such tests should rely on crystal plasticity. That is why, the simulation of the torsion of multicrystals is considered in this work. The stress is laid on a precise description of the intragranular stress and strain fields, which requires an enormous computation effort. Therefore it is resorted to parallel finite element computations. The results presented in this work deal only with small deformations for obvious reasons of computation time so that a direct comparison with the results of [1] will not be possible. The torsion of single crystals is first considered, followed by the torsion of multicrystals and the transition to homogenized polycrystals.

2 TORSION OF SINGLE CRYSTAL BARS

The torsion of f.c.c. metal single crystals is known to give rise to non-homogeneous deformation patterns along the circumference of the specimen [2]. It is simply due to the orientation changes between the stress vector and the fixed crystal orientation, which leads to Schmid factor variation along the circumference. When octahedral slip systems are taken into account, torsion with respect to a [001] axis is associated with the formation of four zones of intense deformation. These zones have been predicted by simulation and observed experimentally in [2] and [3].

Classical crystal plasticity constitutive equations like in [4] are sufficient to interpret and simulate such deformation patterns. Considering plastic deformation according to 12 octahedral slip systems, the plastic strain rate reads in the small deformation framework :

$$\underset{\sim}{\dot{\varepsilon}}^p = \sum_{s=1}^{12} \dot{\gamma}^s \{\underline{\mathbf{l}}^s \otimes \underline{\mathbf{z}}^s\} \tag{1}$$

where $\underline{\mathbf{l}}^s$ is the glide direction and $\underline{\mathbf{z}}^s$ the normal to the slip plane. The brackets denote the symmetric part of the orientation tensor. Plastic flow occurs according to the Schmid law and a viscoplastic formulation of the model is retained in order to get rid of the possible indeterminacy problem for the active slip systems. The amount of slip γ^s on slip system s is given by :

$$\dot{\gamma}^s = < \frac{\mid \tau^s - x^s \mid - r^s}{k} >^n sign(\tau^s) \tag{2}$$

where $\tau^s = \underset{\sim}{\sigma} : \{\underline{l}^s \otimes \underline{z}^s\}$ is the resolved shear stress. An expression for the internal variable r^s of isotropic hardening is :

$$r^s = r_0 + q \sum_r h_{sr}(1 - \exp(-bv^r)) \tag{3}$$

where $\dot{v}^s = \mid \dot{\gamma}^s \mid$. h_{rs} denotes the interaction matrix. The evolution of the kinematic hardening variable is given by :

$$x^s = c\alpha^s \quad \text{and} \quad \dot{\alpha}^s = \dot{\gamma}^s - d\dot{v}^s\alpha^s. \tag{4}$$

In the case of copper, the material parameters have been identified in [4] using tension and cyclic tests :

$$C_{11} = 159310\text{MPa}, C_{12} = 121950\text{MPa}, C_{44} = 80940\text{MPa}$$

$$r_0 = 0.8\text{MPa}, q = 3.6\text{MPa}, b = 1.6, c = 3402\text{MPa}, d = 3597$$

$$h_{ii} = 1, h_{12} = 4.4, h_{13} = h_{14} = h_{15} = 4.75, h_{16} = 5.$$

In the sequel of this work, we consider the torsion of copper cylinder specimens (radius : 1 mm, length 8mm). In this section, only single crystal specimens are studied. Figures 1 to 4 give the non-homogeneous deformation patterns on a section of the specimen when the specimen axis (axis 2) successively coincides with directions [001], [111], [011] and [11$\bar{2}$]. It can be seen that the number and location of intense deformation zones, and the activated slip systems strongly depend on crystal orientations. Note the four, six or two-fold symmetry. The respective torque-displacement curves are given on figure 5. Orientation [001] is seen to be the most resistant one.

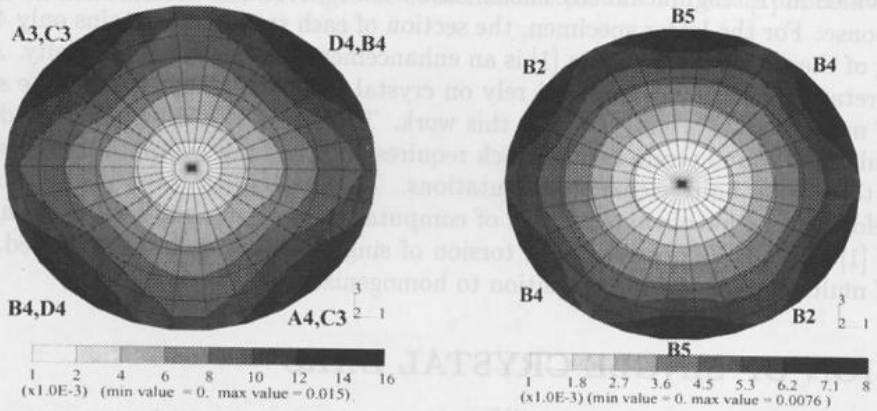

Figures 1 and 2 : Torsion of single crystal bars : equivalent plastic strain in the section (left : axis 2 = [001], axis 1 = [100]; right : axis two = [111], axis 1 = [1$\bar{1}$0]

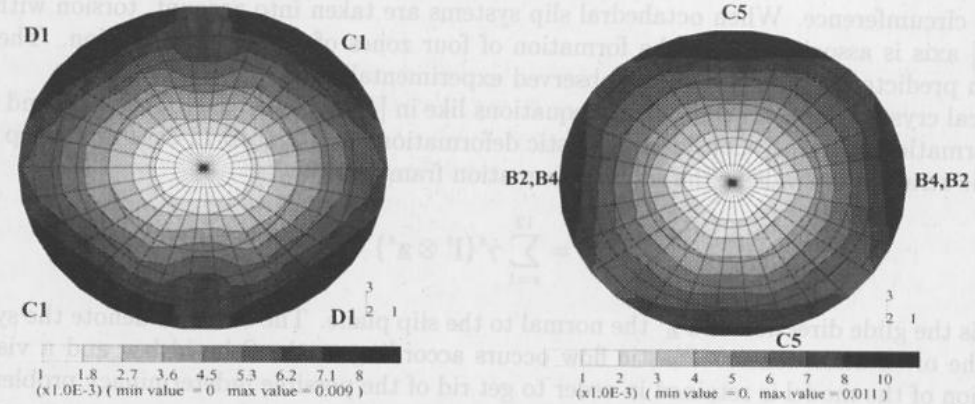

Figures 3 and 4 : Torsion of single crystal bars : equivalent plastic strain in one section (left : axis 2 = [011], axis 1 = [100]; right : axis two = [11$\bar{2}$], axis 1 =[1$\bar{1}$0]

If the specimen axis coincides with a crystal direction lying in the interior of the standard triangle, the deformation patterns are less symmetric and even more complex. This has been shown numerically and experimentally in [3].

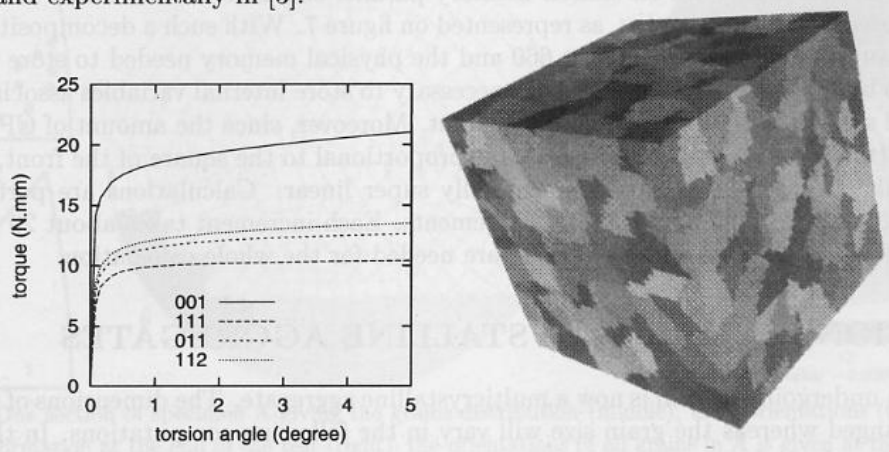

Figures 5 and 6 : Torque-angle curves for various single crystal specimens (left); synthetic polycrystalline aggregate (right).

3 GENERATION OF THE MULTI-CRYSTALLINE TORSION TEST PIECE AND PARALLEL COMPUTING

We use the so-called Multiphase Element technique, where each integration point of the FE mesh is given the particular properties of the grain to which it belongs. More precisely the single-crystal model described in section 2 is used at each integration point with the crystallographic orientation of the corresponding grain in the polycrystalline material. Definition of the microstructure is based upon a synthetic polycristalline aggregate generated by disposing germination points in a cube of unit length and applying an isotropic growth law to obtain an equiaxed microstructure [5]. This synthetic aggregate is obtained in the form a pixel file of resolution 256*256*256, containing grain numbers. For this study we have used an aggregate containing 15583 grains, with about 25 grains in each direction (figure 6 shows a smaller aggregate of 996 grains that has been used in another study).

Test pieces of arbitrary shapes with arbitrary grain sizes can then be generated by placing the FE mesh (scaled down to the appropriate value) inside this cube of polycrystalline material. The FE mesh must be fine enough to account for the strong heterogeneities of the stress and strain fields arising from the torsion loading and this fine modeling of the microstructure. Since we have in mind to vary the number of grains in the cross section of the copper wires, we have generated a finite element model made of 7072 quadratic 20-nodes brick and 15-nodes prismatic elements, for a total of 90141 degrees of freedom. There is about 4000 elements in the section and we can expect enough accuracy for copper wires with up to 50 grains in the section. For such a model the average front, which characterizes the amount of physical memory needed to factorize the global tangent matrix LU form, is of about 4040 corresponding to 2.9 Go of memory. Since conventional sequential computers with enough memory are not commonly available, parallel computing is mandatory for this kind of modeling. The finite element code Zébulon developed at Ecole des Mines de Paris has been parallelized to take advantage of our 6-processors IBM-SP2 distributed memory computer [6]. This parallel implementation is based on the FETI solver (Finite Element Tearing and Interconnecting), developped by F-X Roux at ONERA [7]. In this method the initial mesh is decomposed into sub-domains, and the algorithm consists in searching the solution within each subdomain which minimizes the jump of displacements at the interface between the subdomains, this interface problem being solved by an iterative method (typically the Conjugate Gradient). Once factorized the tangent matrix local to the subdomains, each iteration of the interface solver mainly involves solving the

triangular systems local to each subdomain, and is therefore not too CPU consuming. On the other hand communications are restricted to interface degrees of freedom, which accounts for the good performances of this algorithm on shared memory parallel computers. The initial finite element is thus decomposed into 6 subdomains, as represented on figure 7. With such a decomposition, the front local to each subdomain is now of about 660 and the physical memory needed to store the matrix is of only 80 Mo by processor, leaving the space necessary to store internal variables associated with the 12 octahedral slip systems at each integration point. Moreover, since the amount of CPU needed for factorization (the most CPU consuming step) is proportional to the square of the front, the speedup achieved during parallel computation is generally super linear. Calculations are performed up to about a 5 degree torsion angle in 500 load increments. Each increment takes about 20 minutes on 6 processors of the IBM-SP2, such that 7 days are needed for the whole calculation.

4 TORSION OF MULTICRYSTALLINE AGGREGATES

The specimen undergoing torsion is now a multicrystalline aggregate. The dimensions of the specimen are left unchanged whereas the grain size will vary in the following computations. In the sequel, we will refer to six calculations :

• test A : specimen with 23 grains; • test B : same microstructure as A but a different distribution of orientations (different realization); • test C : 79 grains; • test D : same as C but a different realization of orientation distribution; • test E and F : 332 and 976 grains respectively.

Figures 8 and 9 show the equivalent plastic deformation for the specimens A and C. It appears that for this small number of grains, deformation inevitably tends to localize in one or two sections of the specimen. These particular sections of the specimens are represented on figures 10 and 12 respectively. They contain 6 and 11 grains respectively, the orientation of which are given. Deformation is shown to be very heterogeneous both in the radial direction and along the circumference. The deformation patterns are very similar to those observed in misoriented single crystals under torsion (see section 2). This is particularly clear for a section of specimen B presented on figure 11.

The interesting point is that this special feature of multicrystal deformation under torsion is still observed for greater numbers of grains. Even though 332 and 976 grains are considered in the simulations E and F, deformation is localized within one or two sections (figures 13 to 15). However, localization is less pronounced in the latter case (specimen F). The highly heterogeneous strain field in one section of this specimen is given on figure 15.

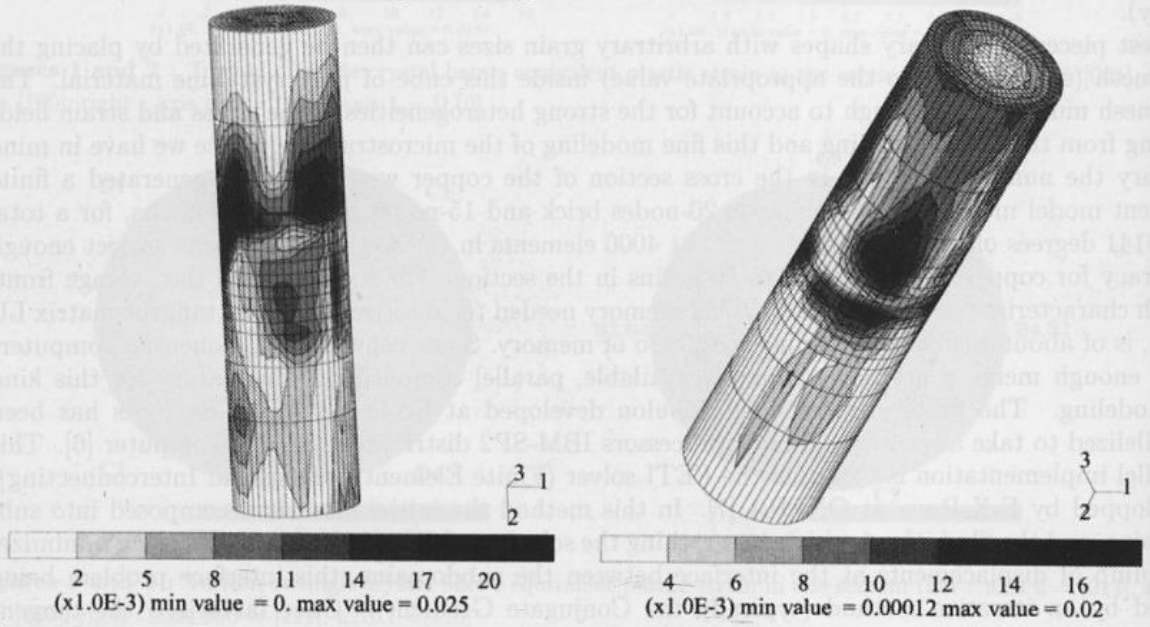

Figures 8 and 9 : Equivalent plastic strain on specimens with 23 (A, left) and 79 (C, right).

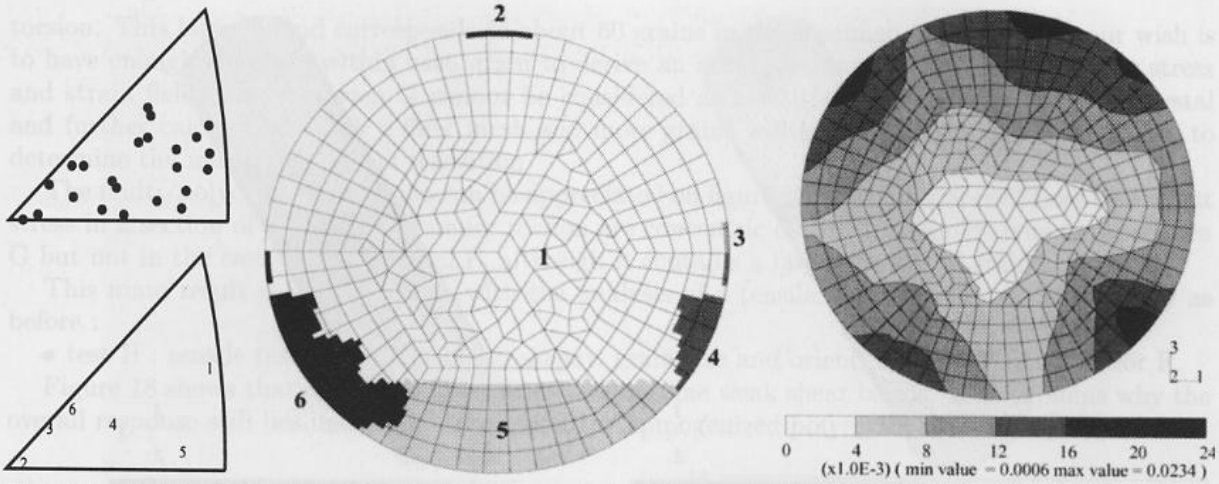

Figure 10 : One section of specimen A giving the grains distribution (middle), their orientations (bottom left) and the plastic deformation at the end of the test (right); the orientations of all grains in A is given at the top left corner (axis 2 in the standard triangle).

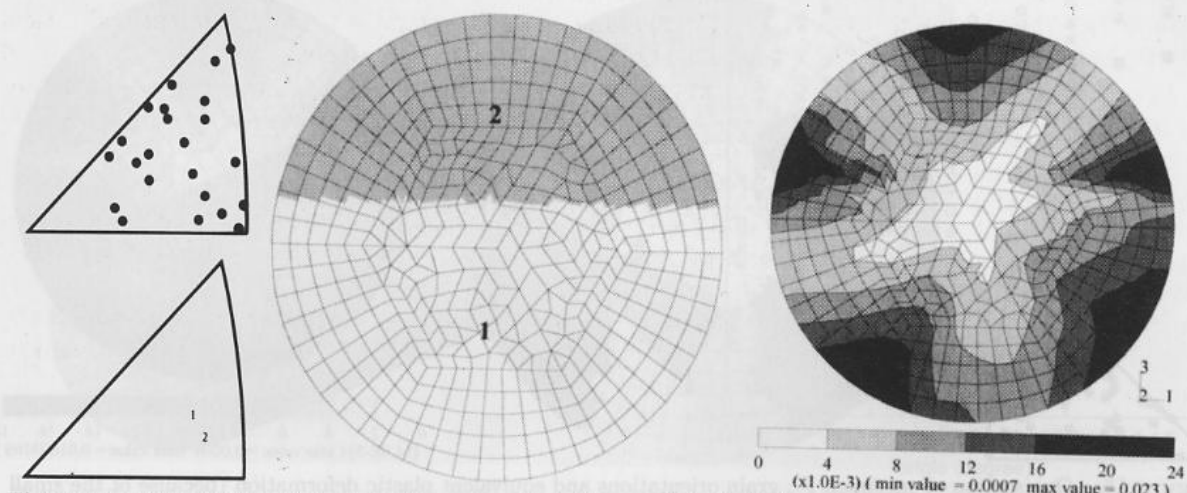

Figure 11 : One section of specimen B : grain orientations and plastic deformation.

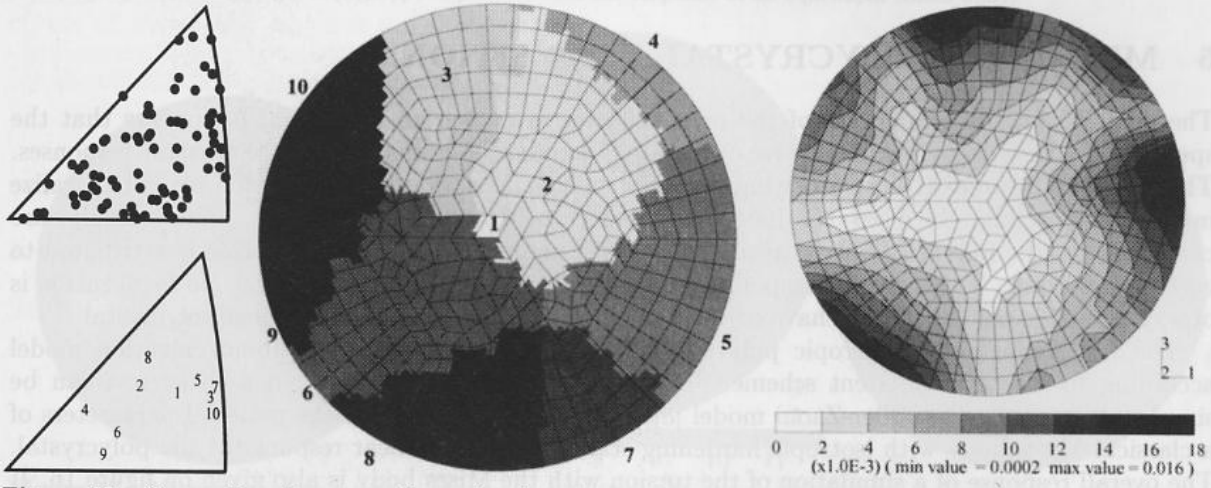

Figure 12 : One section of specimen C : grain orientations and plastic deformation.

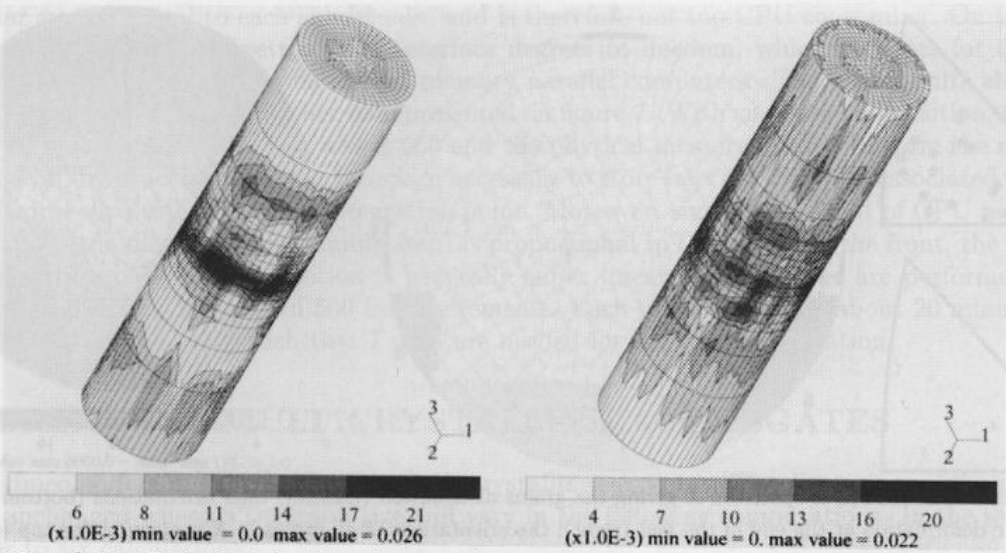

Figures 13 and 14 : Equivalent plastic strain on specimenswith **332** (left) and **976** (right).

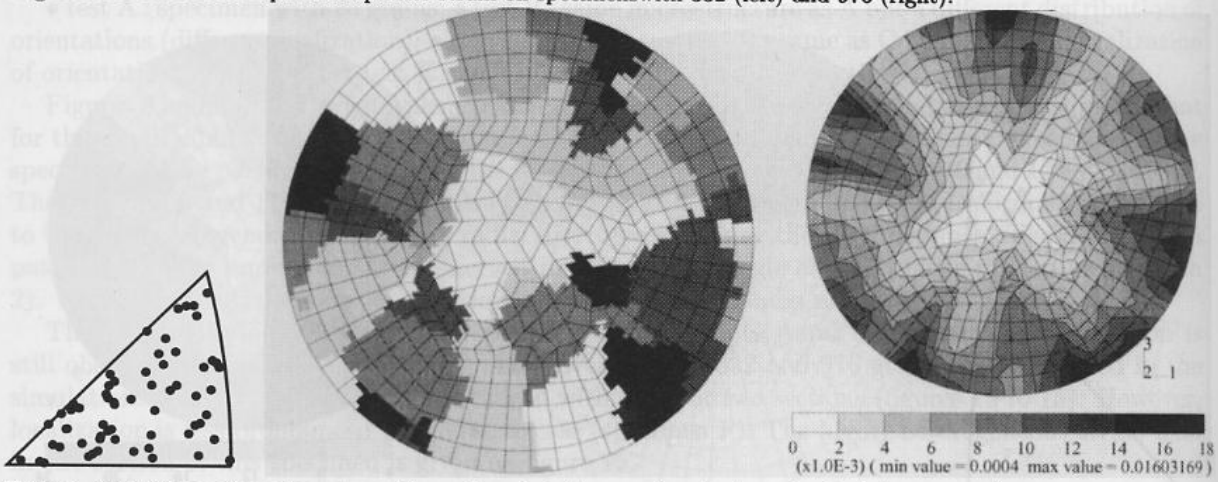

Figure 15 : One section of specimen F : grain orientations and equivalent plastic deformation (because of the small number of colours, all grains cannot be distinguished).

5 MULTI- TO POLYCRYSTAL TRANSITION

The overall torque/angle curves of the previous tests are given on figure 16. It appears that the specimens A,B, C and D which involve only a small number of grains, lead to the weakest responses. This can be interpreted in the following manner : in a chain of grains, deformation tends to localize in the weakest link. In contrast, the tests E and F yield a stronger response. These results are confronted to the following test : • test G : in this specimen, a different orientation is attributed to each Gauss point. The obtained response is found to lie over the previous curve. No localization is observed in this case and the behaviour may be regarded as that of a fine-grained polycrystal.

The behaviour of the isotropic polycrystal can be approximated by a homogenization model according to the self-consistent scheme. The response of the polycrystal to a shear test can be simulated using the Berveiller-Zaoui model [8]. We have then identified the material parameters of a classical Mises body with isotropic hardening starting from the shear response of the polycrystal. The overall response of a simulation of the torsion with the Mises body is also given on figure 16. It almost coincides with that of specimen G. As a result, the maximum number of grains considered in this work (976 grains) is not sufficient to reach the behaviour of the polycrystal. It enables us to establish a lower bound of the critical number of grain for the transition multi/polycrystal under

torsion. This lower bound corresponds to about 60 grains in the specimen section. Since our wish is to have enough elements within each grain to derive an accurate description of intragranular stress and strain fields, the specimen G cannot be considered as a satisfactory model for the polycrystal and further calculations with a finer mesh and more grains will be necessary in the near future to determine the multi/polycrystal transition.

The multi/polycrystal transition can be appreciated on figure 17 : the contours of Mises equivalent stress in a section of a Mises solid under torsion are concentric circles. This holds true for specimen G but not in the case of multicrystal F, although it contains a large number of grains.

This main result is in accordance with the analysis of a tensile test with the same geometry as before :

- test H : tensile test with the same geometry, grain size and orientation distribution as for F.

Figure 18 shows that deformation localizes within some weak shear bands. This explains why the overall response still lies under the response of the homogenized polycrystal (figure 19).

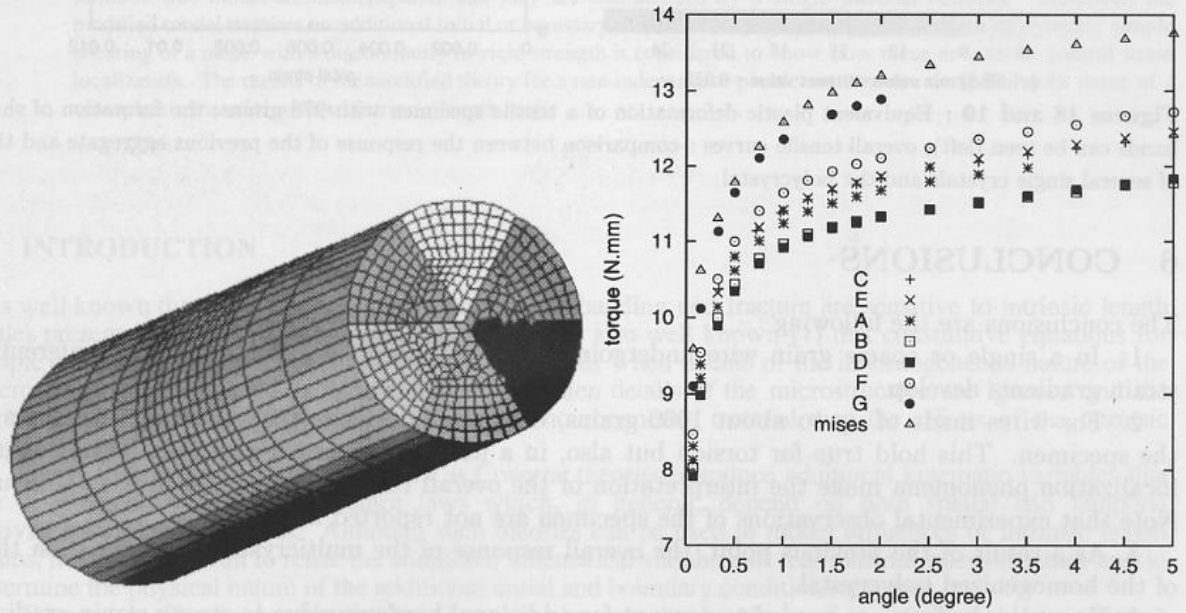

Figures 7 and 16 : Decomposition of the FE model in 6 subdomains (left); torque-angle curves for multicrystalline and polycrystalline aggregates (right); comparison with the response of an equivalent Mises body.

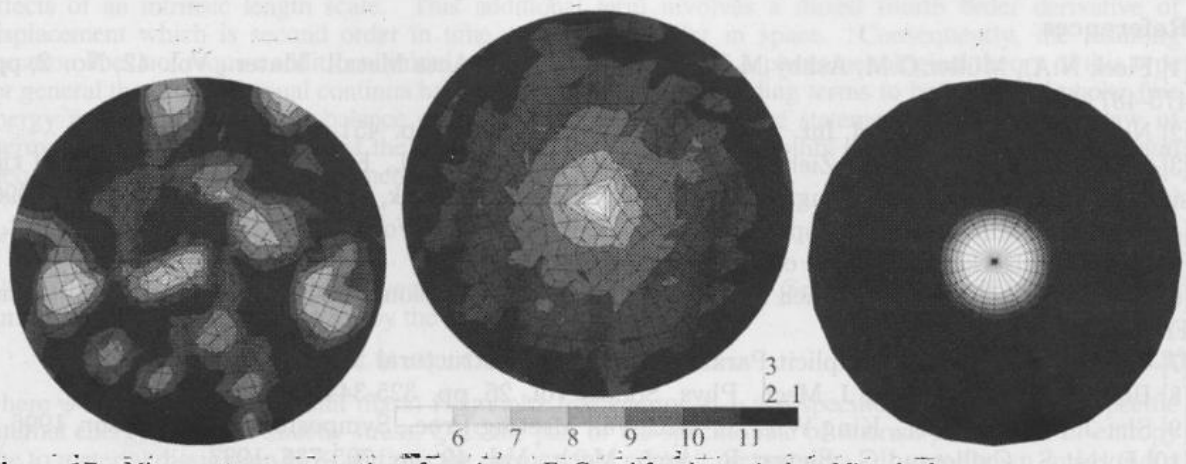

Figure 17 : Mises contour on a section of specimens F, G and for the equivalent Mises body.

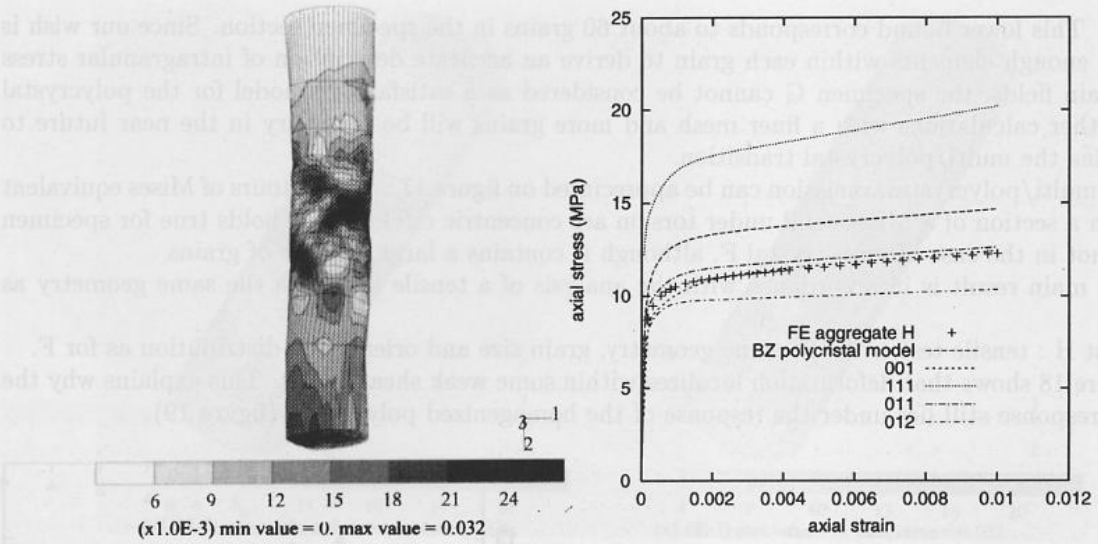

Figures 18 and 19 : Equivalent plastic deformation of a tensile specimen with 976 grains; the formation of shear bands can be seen (left); overall tensile curves : comparison between the response of the previous aggregate and that of several single crystals and the polycrystal.

6 CONCLUSIONS

The conclusions are the following :

1. In a single or coarse grain wire undergoing torsion, both strong radial and circumferential strain gradients develop.

2. For wires made of up to about 1000 grains, deformation localizes in some weak sections of the specimen. This hold true for torsion but also, in a less pronounced manner, in tension. Such localization phenomena make the interpretation of the overall response torque/angle very difficult. Note that experimental observations of the specimen are not reported in [1].

3. As a result of the previous point, the overall response of the multicrystal is weaker than that of the homogenized polycrystal.

4. If non local effects are needed to account for additional hardening due to strong strain gradient in coarse grain wires, this should not be done in an extension of Mises-type elastoplasticity but within the framework of generalized crystal plasticity as in [9] and [10].

References

[1] Fleck N.A., Müller G.M, Ashby M.F., Hutchinson J.W., Acta Metall. Mater., Vol. 42, No. 2, pp. 475-487, 1994.

[2] Nouailhas D., Cailletaud, Int. J. Plasticity, Vol. 11, No. 4, pp. 451-470, 1995 .

[3] Forest S., Olschewski J., Ziebs J., Kühn H.-J., Meersmann J., Frenz H., in Proceedings of the sixth International Fatigue Congress, ed. G. Lütjer ing, H. Nowack, Pergamon, pp. 1087-1092, 1996.

[4] Méric L., Cailletaud G., Gaspérini M., Acta Metall. Mater., Vol. 42, No. 3, pp. 921-935, 1994.

[5] Jeulin D., Decker L., private communication, 1997.

[6] Feyel F., Cailletaud G., Kruch S., Roux F.X., Colloque National en calcul de structures, Giens, France, 20-23 mai 1997.

[7] C.Farhat, F.-X. Roux, Implicit Parallel Processing in Structural Mechanics, 1994.

[8] Berveiller M., Zaoui A., J. Mech. Phys. Solids, Vol. 26, pp. 325-344, 1979.

[9] Shu J.Y., Fleck N.A., King W.E., in MRS Fall Meeting Proc., Symposium W, *to appear*, 1996.

[10] Forest S., Cailletaud G., Sievert R., Arch. Mech., Vol. 49, pp. 705-736, 1997.